

# X-ray diffraction patterns from samples in the laser-heated diamond anvil cell

Wendy R. Panero<sup>a)</sup> and Raymond Jeanloz

*Department of Earth and Planetary Science, University of California, Berkeley, California 94720*

(Received 7 August 2001; accepted for publication 15 November 2001)

Thermal pressure and thermal expansion have competing effects on x-ray diffraction patterns obtained from polycrystalline samples at high pressures (10–100 GPa) and temperatures (300–4000 K) within the laser-heated diamond cell. Modeling shows that realistic temperature and pressure variations within the sample cause systematic shifts in diffraction-line positions and shapes, predicting that inferred values of pressure and thermal expansion coefficient can be off by 0.5%–20% and up to 50%–100%, respectively. Peak splitting due solely to temperature variations within the sample can be spuriously ascribed to the occurrence of a phase transition. The Debye–Waller factor has a systematic effect on diffraction-pattern intensities, but a negligible effect (<0.1%) on line positions except in extreme cases. © 2002 American Institute of Physics.  
[DOI: 10.1063/1.1435837]

## INTRODUCTION

*In situ* high-pressure, high-temperature x-ray diffraction measurements are required for the accurate determination of the pressure and temperature of phase transitions, and pressure–volume–temperature ( $P$ – $V$ – $T$ ) equations of state of crystalline materials. The laser-heated diamond-anvil cell, coupled with x-ray powder diffraction, allows for structural and volume data to be obtained up to several megabar ( $10^{11}$  Pa) in pressure and  $\sim 5000$  K in temperature.

X-ray diffraction measurements with continuous laser heating require a well-aligned system in which the x-ray beam is collinear with either a single- or double-sided laser heating system (Fig. 1). Temperature measurements are made through spectroradiometry,<sup>1</sup> either at a single point or as a function of distance across the sample. These measurements are typically performed along a viewing direction that is co-axial with the beam of the heating laser, and are therefore insensitive to axial variations in temperature. That is, axial gradients are not directly measured, although their magnitudes are often reflected through secondary effects such as broadening of x-ray diffraction lines.

Systematic errors in the determination of the pressure and temperature of a sample inside the laser-heated diamond cell cause significant errors in the measurement of such properties as the coefficient of thermal expansion. An inappropriate assignment of the peak temperature to the x-ray sample volume results in as much as a 100% error in thermal expansion values derived from the experiments, as does a systematic error in the density determination. Here we examine temperature and pressure variations in the laser-heated diamond-anvil cell, and their effects on the x-ray diffraction patterns that are used for determining crystal structures and equations of state.

## TEMPERATURE AND PRESSURE VARIATIONS IN THE LASER-HEATED DIAMOND-ANVIL CELL

Changing the temperature of the sample affects the observed x-ray diffraction lines through thermal expansion of the crystal lattice, shifting diffraction lines to larger inter-atomic spacings. However, the thermal expansion coefficient,  $\alpha$ :

$$\alpha = \left( \frac{\partial \ln V}{\partial T} \right)_P \quad (1)$$

is defined for constant-pressure conditions, whereas the hot portion of the sample is confined by colder material (e.g., colder portion of the sample; thermally insulating or stress-relaxing medium around the sample; diamond anvils) and can therefore remain at a near-constant volume, resulting in little or no shift of x-ray diffraction lines. Instead, the pressure ( $P$ ) in the hot region increases through thermal pressure,  $P_{\text{th}}$ :

$$P_{\text{th}} = P(T, V) - P(300\text{K}, V) \quad (2)$$

as

$$P_{\text{th}} = \alpha K_T \Delta T \approx \alpha_0 K_{0T} \Delta T, \quad (3)$$

where  $V$  is the unit-cell volume,  $T$  is the temperature,  $\Delta T$  is the difference between  $T$  and ambient,  $K_T$  is the isothermal bulk modulus, and subscript 0 indicates a value at zero pressure [the approximation in Eq. (3) is that the product of thermal expansion and bulk modulus is constant, which is justifiable at elevated temperatures and pressures].<sup>2</sup>

In reality, experiments have shown that neither limit of constant volume nor constant pressure is accurate for samples inside the laser-heated diamond cell.<sup>3</sup> Instead, some degree of both thermal expansion and thermal pressure is found. Therefore, the exact amount of shift of a diffraction line depends on the degree to which the sample is held at constant pressure (maximum shift) versus at constant volume (minimum shift).

<sup>a)</sup>Present address: Department of Geological Sciences, University of Michigan, Ann Arbor, MI 48109-1063; electronic mail: wpanero@umich.edu

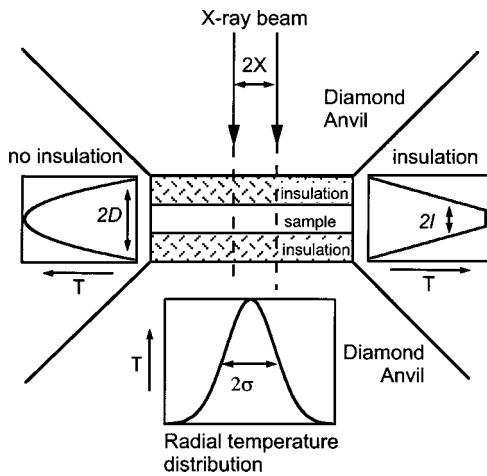


FIG. 1. Schematic cross section of a sample loaded between insulation layers in a laser-heated diamond anvil cell. Diffraction from an x-ray beam (diameter  $2X$ ), aligned colinearly with the beam of a heating laser (waist  $2R$ : not indicated here), is used to determine the lattice parameters of the sample of interest. The resulting temperature distributions are shown. The radial temperature distribution  $[T(r)]$  is similar to that of the radial power distribution in the laser beam, modulated by radial heat flow to give a half-width at half maximum  $\sigma$  [see Eqs. (4) and (5)] (bottom). Axial temperature distributions  $[T(z)]$  are shown on the sides. When using insulation layers, the axial gradients within the sample are reduced (right side). Without the use of insulation layers, the axial temperature distribution is approximately parabolic, dropping to ambient near-temperature at the diamond surfaces (left side). Typical dimensions for such experiments are:  $2D = 10\text{--}30\ \mu\text{m}$ ,  $2l = 1\text{--}20\ \mu\text{m}$ ,  $2X = 5\text{--}20\ \mu\text{m}$ ,  $2\sigma \approx 2R = 30\text{--}100\ \mu\text{m}$ , and total sample diameter of  $50\text{--}500\ \mu\text{m}$ .

If temperature is constant within the x-ray volume, then a well-calibrated internal standard intimately mixed with the sample can be used to constrain the magnitudes of thermal expansion and thermal pressure achieved during laser heating. However, several models of the temperature distribution inside the laser-heated diamond-anvil cell have demonstrated the occurrence of strong temperature gradients across the sample.<sup>4–8</sup>

Laser-heated samples exhibit temperature gradients within the diamond cell for at least two reasons (Fig. 1). First, the power density of absorbed laser light usually varies across the focal spot of the heating-laser beam within the sample. Although use of multiple laser modes can help reduce radial gradients of heating (absorbed laser power) across the hot zone within the sample,<sup>9</sup> heat conduction precludes the complete neglect of radial temperature gradients. Second, because diamond anvils have a large thermal conductivity, the temperature at the diamond-sample interface is approximately ambient, resulting in large axial gradients through the (relatively thin) sample.<sup>4</sup> Thermal-insulation layers are often placed between the sample and diamonds in an attempt to reduce axial temperature gradients. While this can significantly decrease axial gradients within the sample, the use of insulation layers decreases the sample volume, raises the potential for sample contamination (e.g., by chemical reaction with the insulation material),<sup>10</sup> and increases the uncertainty in x-ray geometry. Moreover, temperature gradients tend to become larger with increasing pressure because the sample and insulation layers become thinner, thereby increasing the relative amounts of axial to radial heat conduc-

tion. The magnitude and precise geometry of the temperature variations depend upon the radius of the laser beam, the thicknesses of the sample and any insulation layers, and the specific material properties of the sample.<sup>7</sup>

Temperature variations within the diamond cell can induce pressure variations due to thermal pressure [Eqs. (2) and (3)]. Because of the temperature gradients, each portion of the sample can thus be under different pressure conditions, independent of pressure variations due to material strength and nonhydrostaticity upon loading. Variations in pressure due to laser heating need to be quantified so that x-ray diffraction of a sample under realistic conditions can be interpreted. However, few have closely examined the pressure variations inside the diamond cell due to thermal pressure. Dewaele *et al.*<sup>6</sup> address the specific case of thermal-pressure effects on the phase boundaries of a silica sample in an argon pressure medium, and others (e.g., see Ref. 11) have discussed possible effects of thermal pressure on equation-of-state measurements.

We develop a simple model of steady-state temperature and pressure variations within the (cw) laser-heated diamond-anvil cell. These models apply to samples for which the absorption of the laser beam is assumed constant with thickness. This is approximately true for dielectric samples, either if they are sufficiently transparent (weakly absorbing) or, for more strongly absorbing samples, when laser heated from both sides (from above and below in Fig. 1). Metallic samples absorb the heating laser beam within a thin skin depth, such that the observed radial temperature distribution is more readily interpreted;<sup>5</sup> such samples are therefore not explicitly considered in our general discussion, but because metallic samples are equivalent to highly absorbing samples in the case of double-sided heating and very small thicknesses ( $l \ll D$ ) our analysis can still apply.

Assuming a  $\text{TEM}_{00}$  (gaussian) mode for the heating laser, the resulting radial temperature distribution is approximately gaussian and the axial variation is approximately parabolic.<sup>4,5,7,8</sup> For a sample having constant thermal conductivity and no insulation, the half-width of the radial temperature profile at half the peak temperature [half width at half maximum (HWHM)]<sup>8</sup> is

$$\sigma = R(0.88 + 0.98\sqrt{D/R}) \quad (4)$$

where  $2R$  is the beam waist of the heating laser, and  $2D$  is the gasket thickness (Fig. 1). For the case of a sample with insulation layers, the width of the hotspot is only slightly greater

$$\sigma = R(0.88 + 0.98\sqrt{D/R})[1.078 - 0.078(l/D)], \quad (5)$$

where  $2l$  is the sample thickness. These relations are slightly modified for a sample with thermal conductivity inversely proportional to temperature, as is typical for dielectric materials.<sup>7</sup>

For no insulation layers and constant thermal conductivity, the complete temperature distribution is approximately

$$T(r, z) = (T_m - T_0)e^{-(r/\sigma)^2} [1 - (z/D)^2] + T_0, \quad (6)$$

where  $T_m$  is the peak temperature (i.e., the highest temperature of the three-dimensional hotspot),  $T_0$  is the ambient tem-

perature,  $z$  is the axial dimension, and  $r$  is the radial dimension. For the case of insulation layers and no axial gradients within the sample

$$T(r, z) = (T_m - T_0)e^{-(r/\sigma)^2} + T_0 \quad |z| < l, \quad (7a)$$

$$T(r, z) = (T_m - T_0)e^{-(r/\sigma)^2} \left( 1 - \frac{(|z| - l)}{(D - l)} \right) + T_0 \quad |z| > l. \quad (7b)$$

To generalize the discussion of temperature and pressure variations within the hotspot, the hotspot radius, sample thickness, temperature, and thermal pressure can be expressed in nondimensional terms as

$$\rho = r/\sigma, \quad (8a)$$

$$\zeta = z/D, \quad (8b)$$

$$\tau = (T - T_0)/(T_m - T_0), \quad (8c)$$

$$p = P_{th}/K_{0T}. \quad (8d)$$

Assuming no stress relaxation within the hot zone of the sample, the nondimensional thermal pressure [Eq. (3)] and temperature [Eq. (6) (no insulation) or Eq. (7) (with insulation layers)] for constant thermal conductivity are

$$p(\tau) = \alpha_0(T_m - T_0)\tau, \quad (9)$$

$$\tau(\rho, \zeta) = \exp(-\rho^2)(1 - \zeta^2) \quad (\text{no insulation}), \quad (10a)$$

$$\tau(\rho, \zeta) = \exp(-\rho^2) \quad (\text{insulation; } |\zeta| < l/D), \quad (10b)$$

$$\tau(\rho, \zeta) = \exp(-\rho^2) \left( 1 - \frac{\zeta - 1/D}{1 - l/D} \right) \quad (\text{insulation; } |\zeta| > l/D). \quad (10c)$$

The thermal pressure is approximately linear with temperature at high temperatures; under these conditions, the actual pressure in the sample varies linearly with temperature only to the degree that the sample remains at constant volume during heating.

Figure 2 shows temperature ( $\tau$ ) and maximum thermal pressure ( $p$ ) contours for a sample assembly with constant thermal conductivity, assuming typical values of  $\alpha_0 = 10^{-5} \text{ K}^{-1}$  and  $T_m = 2500 \text{ K}$ , both for a sample with (right) and without insulation layers (left). The former, exhibiting no axial gradients in the sample, is an idealization of a sample that is well insulated from the diamonds and is realistic only for very thin ( $l \ll D$ ) and sufficiently absorbing samples heated from both sides.<sup>12</sup>

With the usual (along-axis) technique of measuring temperature by spectroradiometry, the observed gray-body radiation is obtained from all levels across the full thickness of a dielectric sample, yielding a Planck-like spectrum at an apparent temperature slightly lower than the true peak temperature:<sup>5</sup> a small, but systematic effect [Fig. 2(a)]. As blackbody radiation collected from optically thin samples is dominated by thermal emission from the hottest portions of the sample, the temperatures measured from either side of a semitransparent insulated sample are not representative of the temperature of the sample surface, but of nearly the hottest portion of the sample. Thus, differences in temperature

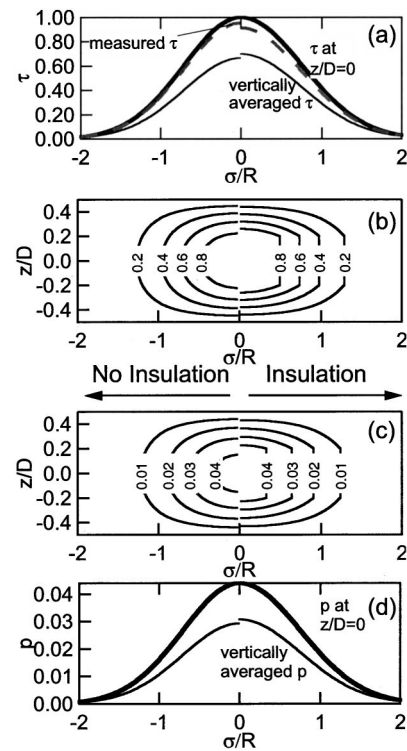


FIG. 2. Contour plots of normalized temperature  $\tau$  (b) and thermal pressure  $p$  (c), and corresponding profiles [(a) and (d), respectively], for samples in the laser-heated diamond anvil cell calculated assuming a cw heating laser operating in TEM<sub>00</sub> mode. The left side ( $\sigma/R < 0$ ) of each panel is calculated for a sample with no insulation layers [Eq. (6)], and the right side ( $\sigma/R > 0$ ) for a strongly absorbing sample of thickness  $l = 0.3D$  heated from both sides. Note that the effect of the insulation layers is to broaden the hotspot radially by about 7%. A comparison between the maximum value, at  $z/D = 0$  (heavy solid curve), and the vertically averaged values (thin solid curve) in panels (a) and (d) indicates that both radial and axial variations in pressure and temperature affect x-ray diffraction measurements. An experimental complication for optically thin samples is that the effect of the axial temperature gradients is to produce a blackbody spectrum having contributions from the full thickness of the sample [dashed curve in (a)], such that the measured temperature is 3%–6% lower than the actual peak temperature distribution at  $z/D = 0$ .

measurements made from the two sides cannot be taken as an indicator of axial temperature gradients under such conditions.<sup>13</sup>

Temperature gradients within the x-ray diffraction volume act to lower the average temperature of the volume below that of the peak temperature value. In fact, these lower temperatures tend to dominate the x-ray diffraction volume because of the cylindrical symmetry of the temperature profiles (i.e., greater areal or volume contribution from cooler regions of the sample, at large radius from the center of the hot spot).<sup>14</sup> This is in contrast with the weighting of the sample's blackbody spectrum toward the peak temperature, as just noted. The sample temperature to which the x-ray diffraction is most sensitive thus depends on the ratio of the x-ray spot size (diffraction-volume radius) to the characteristic dimension of the radial temperature distribution; the effect of axial gradients is largely independent of the x-ray beam diameter. Therefore, it is the volume-average temperature in the part of the sample probed by the x-ray beam (not the temperature of the sample's average blackbody emission)

TABLE I. Models considered for calculating peak shapes.

Temperature conditions considered			$P-V$ cases	
I	$X = \sigma$	perfect insulation	A	Constant volume
II	$X = \sigma/4$	perfect insulation	B	Constant pressure
III	$X = \sigma$	no insulation	C	Volume and pressure intermediate
IV	$X = \sigma/4$	no insulation		

that should be used to interpret diffraction patterns obtained from the laser-heated diamond cell.

### EFFECT OF TEMPERATURE DISTRIBUTION ON X-RAY DIFFRACTION PEAK SHAPES

The focus of the present study is on the effects of realistic temperature distributions on high-pressure x-ray diffraction patterns. Consequently, the models presented here neglect sample-dependent diffraction effects that are independent of temperature, such as atomic scattering factors and the absorption of x rays by the sample. We also ignore experimental complications such as temporal fluctuations in temperature, misalignment of the laser-heating spot with the center of x-ray diffraction, variations in sample thickness, or complications with the precision and accuracy of measuring temperatures and temperature gradients.

We model four different geometries of laser-heating with x-ray diffraction (Table I): “perfect” insulation layers versus no insulation, as indicated in Fig. 1, and a relatively large hotspot ( $\sigma = 4X$ ) versus a narrow hotspot ( $\sigma = X$ ). These represent extremes in temperature gradients, from strong to virtually none. For the extreme of a sample with no insulation layers, large axial temperature gradients are obtained within the sample,  $T'(z)$  (prime indicates differentiation with respect to the indicated coordinate) (Fig. 1, left). However, the lack of insulation layers can serve as an advantage, because the temperature variations can be modeled precisely, given just the peak temperature and the thickness of the sample (measured from the gasket thickness after the experiment).<sup>8</sup> While this geometry may not be ideal for use in a  $P-V-T$  equation of state measurement, it does allow for a better constraint on the actual temperature variations within the x-ray diffraction volume than when insulation layers are present (as these layers require extra modeling).

At the other extreme, samples with perfect insulation are modeled as having no axial temperature gradients (Fig. 1, right). Insulation layers often have variable thickness and the layers on either side of the sample may differ in thickness, especially when considering insulation layers loaded as a fluid (e.g., Ar, Ne). With increasing pressure, the sample thins, which facilitates axial heat conduction; thus, an increase in pressure generally increases both radial and axial temperature gradients,  $T'(r)$  and  $T'(z)$ .<sup>7</sup> Also, traditionally chosen insulation or pressure-medium layers (e.g., NaCl, Ar, He) tend to be more compressible than the sample of interest, so that the insulation layers thin more rapidly than the sample with increasing pressure. This results in the occurrence of significant temperature- and pressure-dependent

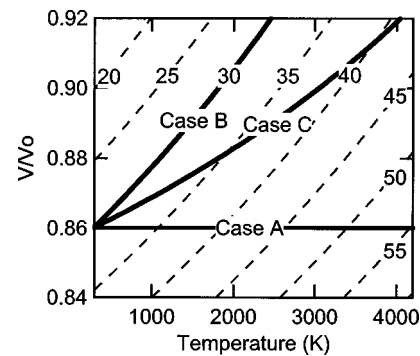


FIG. 3. Pressure (dashed contours, in GPa) as a function of volume and temperature calculated for gold at an initial pressure of 20 GPa. The three  $P-V$  conditions considered in the present models, A, B, and C, are shown. For a given case, each point in the x-ray volume can be found along the curves as indicated; the only variable (for a given material and peak temperature) is then the pressure at 300 K.

axial gradients across the sample. Therefore, models that ignore axial temperature gradients (Fig. 1, right side), should be taken as an idealization.

The x-ray beam used in the experiment is collimated or focused to a size comparable to, and preferably much smaller than, the diameter of the laser-heated spot. With increasing pressure, however, a thinner sample has a small hotspot, such that the ratio of the hotspot size ( $\sigma$ ) to the x-ray spot size ( $X$ ) typically decreases with increasing pressure for a given sample, regardless of the insulation that is used.<sup>8</sup> Consequently, in addition to modeling the effects of two extremes in axial gradients, we also model the effects of variations in radial gradients (Table I).

When laser heated, the pressure in the sample changes in response to thermal pressure and to stress relaxation of the sample and surroundings (e.g., pressure medium and gasket); the measured unit-cell volumes correspondingly change in response to thermal expansion and pressure relaxation of the sample. Because of the competing effects of thermal expansion (at  $\sim$ constant pressure) and thermal pressure (at  $\sim$ constant volume), the precise  $P-V$  conditions are not known *a priori*. Therefore, temperature and unit-cell volume of a standard must be measured in order to determine the pressure of the sample throughout the heating cycle [e.g., see Ref. 3].

Here we consider three different  $P-V$  paths in order to model diffraction patterns obtained during laser heating of samples inside the diamond cell (Table I, Fig. 3): (A) constant-volume (“rigid container”) conditions, in which the lattice parameters of the sample remain constant upon heating; (B) constant-pressure conditions, in which the unit-cell volume increases with increasing temperature at each point across the sample according to the thermal expansion of the material; and (C) an intermediate case in which the thermal energy is split between increasing the pressure and expanding the volume of the sample. Specifically, at each point in the x-ray volume the unit-cell volume of the material of interest is defined by

$$V(T, P) = V(300K, P_0) + 1/2[V(T, P_0) - V(300K, P_0)], \quad (11)$$

TABLE II. Thermoelastic properties of materials considered.

	Pt	Au	MgO	Diamond	NaCl
$V_0$ (Å <sup>3</sup> )	60.38 <sup>b</sup>	67.83 <sup>d</sup>	74.67 <sup>e</sup>	45.38 <sup>f</sup>	179.22 <sup>h</sup>
$\Theta$ (K)	230 <sup>c</sup>	170 <sup>d</sup>	945 <sup>e</sup>	2230 <sup>g</sup>	304 <sup>i</sup>
$K_{0T}$ (GPa)	278 <sup>b</sup>	167 (6) <sup>d</sup>	162.5 (0.2) <sup>e</sup>	444 (3) <sup>f</sup>	23.8 (7.5) <sup>h</sup>
$K_T$	5.6 <sup>b</sup>	5.48 (0.54) <sup>d</sup>	4.13 (0.09) <sup>e</sup>	1.9 (0.3) <sup>f</sup>	4 (3.9) <sup>h</sup>
$\gamma$	2.4 (0.5)	2.95 (0.43) <sup>d</sup>	1.54 <sup>e</sup>	1 <sup>a</sup>	1.59 (0.04) <sup>i</sup>
$q$	1.5	1.7 (0.7) <sup>d</sup>	1 <sup>a</sup>	1 <sup>a</sup>	1 <sup>a</sup>

<sup>a</sup>Assumed value.

<sup>b</sup>See Ref. 20.

<sup>c</sup>See Ref. 18.

<sup>d</sup>See Ref. 21.

<sup>e</sup>See Ref. 22.

<sup>f</sup>See Ref. 23.

<sup>g</sup>See Ref. 26.

<sup>h</sup>See Ref. 24.

<sup>i</sup>See Ref. 25.

where  $P$  is the actual pressure at that point, and  $P_0$  is the pressure given isobaric conditions.

Case A is trivial, as there is no shift in x-ray diffraction peaks or shapes. Case B is extreme in assuming complete stress relaxation and is generally not observed in experiments.<sup>3</sup> Therefore, case C is the most representative of typical experimental conditions, although it must be recognized that states can range between A and C not only from one experiment to the next but even within a single heating cycle during one experiment.

For each of the four geometries of temperature distribution, we model five simple materials having cubic unit cells: Au, Pt, MgO, NaCl, and diamond. These materials are commonly used as internal standards [e.g., see Ref. 15], and represent extremes in thermal expansion and compressibility (NaCl and diamond) (Table II).

Throughout our analysis, the pressure–volume–temperature relationships are defined by a Mie–Grüneisen equation of state, [e.g., see Ref. 2]:

$$P(V, T) = \frac{\gamma}{V} [E_{th}(T, \Theta) - E_{th}(300K, \Theta)] + P_{300}(V), \tag{12}$$

where  $\Theta$  is the Debye temperature and  $\gamma$  is the Grüneisen parameter. The thermal energy,  $E_{th}$ , is determined through the Debye approximation ( $n$  is the number of atoms per chemical formula unit,  $R$  the gas constant,  $x$  is  $\Theta/T$ ):

$$E_{th}(T, \Theta) = \frac{9nRT}{x^3} \int_0^x \frac{\xi^3}{e^\xi - 1} d\xi \tag{13}$$

and  $P_{300}(V)$  is determined by the third-order eulerian finite-strain (Birch–Murnaghan) equation of state

$$P_{300}(V) = 3K_{0T}f(1 + 2f)^{5/2} [1 - \frac{3}{2}(K' - 4)f], \tag{14}$$

where

$$f = \frac{1}{3} [(V_0/V)^{2/3} - 1] \tag{15}$$

and  $K_{0T}$  is the zero-pressure isothermal bulk modulus (with pressure derivative  $K'$ ). As before,  $V$  is the unit cell volume

at  $P$  and  $T$ , and  $V_0$  is the volume at zero pressure and 300 K. The Debye temperature and Grüneisen parameter are taken to be only functions of volume

$$\gamma = - \frac{d \ln \Theta}{d \ln V} \tag{16}$$

and

$$q = \frac{d \ln \gamma}{d \ln V} \tag{17}$$

such that

$$\Theta = \Theta_0 \exp \left\{ \frac{\gamma_0 [(V/V_0)^q - 1]}{q} \right\}. \tag{18}$$

For each point in the x-ray diffraction volume, the portion of the sample intersected by the x-ray beam, it is therefore possible to calculate iteratively a unit-cell volume given  $T(r, z)$ , material properties (Table II), and assumptions on the pressure conditions of the sample according to the curves in Fig. 3. For all cases but constant-volume conditions, the resulting x-ray diffraction peaks are shifted, changing in shape and location due to the temperature variations. Because the geometry of the temperature distribution is such that a greater portion of the x-ray diffraction volume is at lower temperatures than at the peak temperature, calculated diffraction peaks should have asymmetries reflecting the actual temperature distribution within the x-ray volume.

For purposes of illustration, diffraction-peak shapes are calculated assuming a relatively high resolution, or narrow isothermal peak profile, of  $\delta d/d = 0.15\%$ , where  $d$  is the interplaner spacing. This profile is representative of the peak widths observed for hydrostatic samples using angular dispersive diffraction onto image plates, assuming a typical experimental geometry of a 25 cm sample-to-film distance and an image plate resolution of 50  $\mu\text{m}$ . Decreased resolution (wider isothermal peaks) simply smears out the peaks obtained at high temperatures.

The contrast between constant-pressure (case B; black curves) and constant-volume conditions (case A; gray curves) is illustrated in Figs. 4(a)–4(e) for each material of

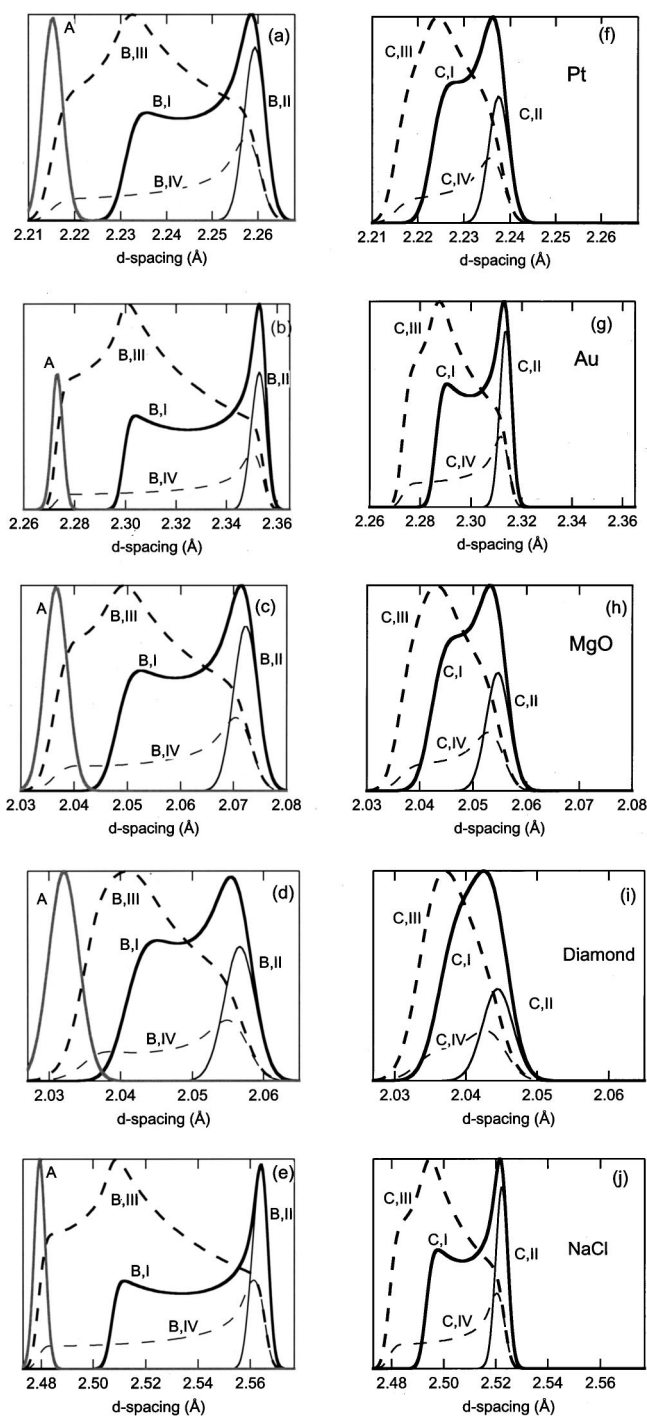


FIG. 4. Predicted diffraction-peak shapes for each material listed in Table II, assuming (a)–(e) constant-volume (gray curves: case A) or constant-pressure conditions (black curves: case B), or (f)–(j) intermediate conditions (case C). An initial pressure of 20 GPa and a peak temperature of 3000 K are assumed, and labels on the curves indicate the  $P$ – $V$  case and temperature conditions according to Table I: Bold lines indicate  $X = \sigma$  (conditions I and III), thin lines indicate  $X = \sigma/4$  (conditions II and IV), dashed lines indicate no insulation layers (conditions III and IV) and solid lines indicate perfect axial insulation (conditions I and II). All profiles are calculated assuming an isothermal peak width (HWHM) of  $0.003 \text{ \AA}$  ( $\delta d/d = 0.15\%$ ). The diffraction peaks shown are the 100% intensity line for each material ([111] for Au, Pt, and C; [200] for MgO and NaCl). While the temperature and pressure conditions are above the melting point for some of the materials, they represent the expected range of behavior for studies with the laser-heated diamond-anvil cell. Pressures at the hotspot center are 20 GPa for all samples under constant-pressure conditions (case B). Central pressures are 38, 37, 28, 38, and 31 GPa, respectively, for Au, Pt, NaCl, diamond and MgO under constant-volume conditions (case A).

Table II under each of the four temperature conditions of Table I. For specificity, these are calculated assuming a peak temperature of 3000 K and an initial pressure of 20 GPa. Under constant-volume conditions, the patterns are unaffected by thermal expansion so that there is no effect due to the temperature gradients: neither change in position or shape takes place, even with extremely large temperature gradients. However, the sample pressure is very different in the two cases, A and B, and depends on the temperature distribution for constant-volume conditions (the peak pressure is 48 GPa in the latter instance for Au: Fig. 3). Figures 4(f)–4(j) shows the predicted peak shapes for the intermediate case (case C). Here, the pressure is 20 GPa for those portions of the sample at 300 K, and higher (due to thermal pressure) for portions of the sample at higher temperatures.

With the exception of those peaks reflecting negligible temperature variations (e.g., small x-ray beam and insulated sample: II of Table I), all peaks show significant deviations from gaussian for either constant-pressure (B) or intermediate (C)  $P$ – $V$  conditions. Notably, for a sample without any axial gradients, a large-radius diffraction volume with  $X = \sigma$  (temperature condition I) results in a diffraction line with a distinct shoulder—even for diamond, the material with the lowest thermal expansion. The apparent splitting of the diffraction peak results from the combined effects of (i) the  $T(z, r)$  temperature variations, with significantly more signal coming from the lower- than the higher-temperature portions of the sample; and (ii) a thermal expansion coefficient rapidly changing with temperature, as implied by Eqs. (12) and (13). The diffraction peak is dominated by contributions from the edges of the sample and from where the coefficient of thermal expansion is not changing as rapidly.

The resulting peak shapes may lead to incorrect interpretations of data. For example, the shoulder could be interpreted as indicating that the sample undergoes a high-temperature phase transition that does not quench to room temperature (e.g., as might be expected for a displacive transition). In fact, indications of an orthorhombic phase of iron reported at about 45 GPa and 2100 K,<sup>16</sup> and not seen at room temperature, could instead be attributable to thermal expansion effects in a sample with significant temperature variations. In these experiments, a diffraction-line splitting of  $\delta d/d \sim 1.9\%$  was observed from an insulated Fe foil that was laser heated from one side only, with a  $\sigma/X \approx 1$ . Assuming a linear temperature gradient through the sample, where the unheated side of the foil is 60% of the laser-heated side,<sup>5</sup> a gaussian radial temperature distribution with  $X = \sigma$  and pressure-volume case C produces a splitting of 1.8%, approximately the observed splitting. This calculation requires numerous assumptions; though plausible, without published measurements of peak temperatures and radial temperature gradients of the sample, it is impossible to provide a better estimate.

While these findings are troubling, no evidence for such odd profiles as shown in Fig. 4 have been reported to date. Peak widths obtained from energy-dispersive x-ray diffraction systems are 3–5 times wider than assumed in the present models (due to limited energy resolution of current detectors). However, when resolution improves—with the use of

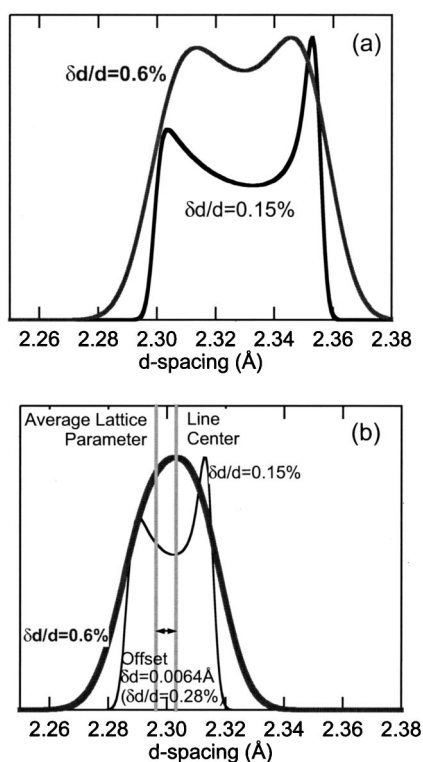


FIG. 5. Predicted peak shapes for the [111] line of gold at 20 GPa determined with a detection system having lower resolution than shown in Fig. 4,  $\delta d/d=0.6\%$  (gray) compared to  $\delta d/d=0.15\%$  (black), for temperature condition I. Models are for (a) constant-pressure conditions (case B), and (b) half the maximum thermal expansion (case C). In the latter case, the center of the peak (right-hand gray bar), corresponding to a compression  $V/V_0=0.954$ , indicates a pressure of 24.0 GPa for a volume-average temperature of 2006 K. The average of the actual sample pressure is 25.5 GPa, corresponding to a compression of  $V/V_0=0.927$  (left-hand gray bar), leading to a 1.5 GPa underestimate of pressure.

high-resolution image plates, for instance—the peak shapes derived in the present study should be observable. Figure 5 shows the effect of lower resolution on the predicted diffraction pattern for gold. In the case of no thermal pressure (B), some effect on the peak shape is evident [Fig. 5(a)]. Still, because constant-pressure conditions are unrealistic, it is reasonable that such results have not been reported. Indeed, for conditions intermediate between maximum thermal pressure and maximum thermal expansion (C), the diffraction lines no longer appear split [Fig. 5(b)].

The lack of diffraction-peak broadening in certain experiments has been cited as evidence for minimal temperature variation within the x-ray volume.<sup>17</sup> To the degree that the sample remains at constant volume, however, this argument is not valid; more generally, it needs to be critically evaluated relative to the resolution of the detection system. Figures 4 and 5 show that the position and width of each diffraction peak are determined both by the temperature variation across the sample and by the specific  $P-V$  path followed upon heating. As one example, assuming temperature condition I, the diffraction-peak width for gold decreases from  $0.029 \text{ \AA}$  ( $\delta d/d=1.4\%$ ) in case B (constant pressure) to  $0.015 \text{ \AA}$  ( $\delta d/d=0.38\%$ ) in case C and  $0.003 \text{ \AA}$  (i.e., the detector resolution;  $\delta d/d=0.15\%$ ) in case A (constant volume). The same studies that cite lack of peak broad-

ening as evidence for minimal temperature variations also must invoke significant thermal pressure, either to reconcile extreme thermal expansion values or to correct the internal-standard pressure. However, an increase in pressure due to heating requires that the volume of the cell is constrained, restricting thermal expansion and therefore, the width of the peak. Even with the best possible resolution of an energy-dispersive x-ray system, these effects are smeared out such that only broadening is observed, with the non-Gaussian signal significantly suppressed. Therefore, the lack of broadening of a diffraction peak does not necessarily demonstrate the lack of temperature gradients if there is any evidence of thermal pressure.

Complicating these arguments is the fact that even though the bulk of the sample seems to follow a particular  $P-V-T$  path upon heating (intermediate between isochoric and isobaric conditions), there is no reason to expect that each point across the sample volume behaves the same way: the coldest portions of the cell do not undergo the same relaxation as the heated portions. Intergranular stresses broaden the peak widths but have been shown to relax when heated to high temperatures,<sup>3</sup> whereas lower-temperature portions of the sample are likely to retain much of this stress. Temperature- (and therefore position-) dependent stress relaxation can thus bias the peak widths toward those portions of the sample that are colder, further tending to shift the observed peak position while smearing out the peak shape.

#### INFERRED PRESSURES OF SAMPLES: IMPLICATIONS FOR $P-V-T$ EQUATIONS OF STATE

Because of the uncertainty of the  $P-V-T$  path followed by the sample during laser heating, experiments require the incorporation of a well-calibrated internal standard that can be assumed to experience the same pressure and temperature conditions as the sample. Thus, any high-pressure, high-temperature equations of state must be measured *relative* to that of a well defined standard. In general, the maximum temperature that is measured or some average temperature of the diffraction volume is taken to be the temperature representative of the measured diffraction pattern, and it is assumed that the sample of interest experiences the same pressure-temperature environment as the internal standard. However, the center of the diffraction peak expected for the volume-average temperature under the conditions defined in Eq. (11) (case C of Table I), is not the center of the calculated peak shape. There is a significant offset because the average expansion across the temperature distribution is not the same as the expansion derived for the average temperature. This difference introduces systematic biases in the inferred pressure, such that the measured pressure from an internal standard is typically less than the actual pressure.

Recent experiments have noted a discrepancy between data collected through different *in situ* techniques: results from the multianvil press and laser-heated diamond anvil cell have been shown to imply a 2–3 GPa difference in inferred phase boundaries,<sup>13</sup> as well as inconsistent determinations of thermoelastic properties.<sup>17</sup> Several explanations have been suggested to explain these differences, from uncertainties in

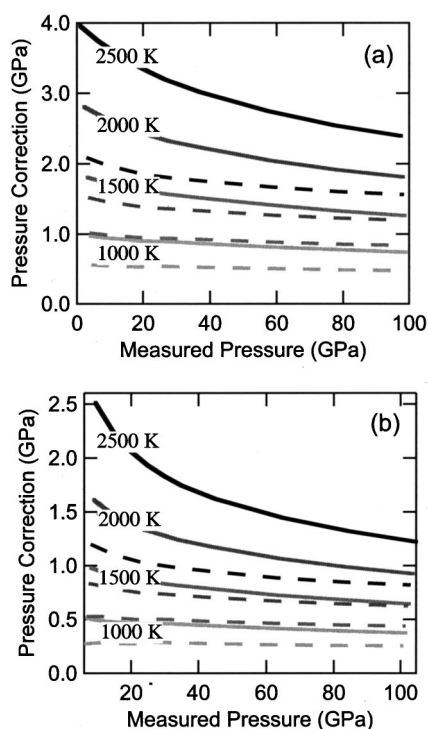


FIG. 6. Correction to the pressure inferred from the diffraction pattern required in order to obtain the actual pressure of the sample for  $X=\sigma$  under (a) constant-pressure conditions, and (b) conditions intermediate between constant pressure and constant volume (case I, C). Solid curves are for gold, and dashed are for MgO. Black is for a volume-average temperature of 2500 K, and shades of gray are for 2000, 1500, and 1000 K.

the thermal equation of state of the internal standard to the presence of nonhydrostatic stresses.

As observed in Fig. 5(b), however, the lattice parameter inferred from the center of the strongest diffraction peak for gold is systematically larger than the actual average lattice parameter (by  $\delta d/d=0.28\%$ ), hence, the pressure that would be inferred is lower than the actual average pressure of the sample. The difference in measured and actual pressure is approximately the same magnitude as the uncertainties in pressure due to uncertainties in temperature and in the equation of state of the internal standard. These systematic effects can result in an incorrect determination of a phase boundary or the pressure derivatives of thermodynamic parameters.

Figure 6 shows the pressure correction required in order to obtain internally consistent results, given the particular  $P-V$  conditions of the sample and the temperature distribution across the x-ray volume. With some indication of the sample condition, between constant-volume and constant-pressure, the appropriate systematic correction can be applied to the pressure calculated from a gaussian fit to the diffraction peaks. Although small, this correction can help explain the difficulties in determining relative equations of state between well-studied materials. For example, at high temperatures (volume average temperature of 2000 K), a well-insulated sample of gold and MgO at 20 GPa (constant-pressure conditions) should indicate pressures of 17.5 and 18.6 GPa, respectively. This is not only a difference of pressure between the sample and standard of 1.1 GPa, but also

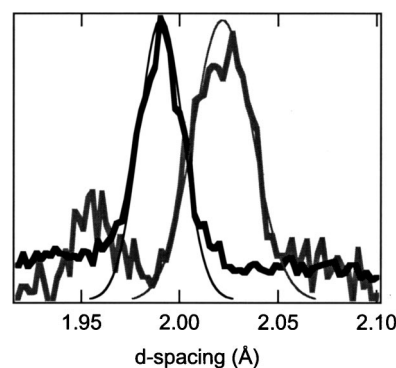


FIG. 7. Diffraction-peak profiles for two samples contained between MgO insulation layers, with peak temperatures of 2150 ( $\pm 75$ ) K in both cases. Gray bold line is for data collected from a sample heated using a TEM<sub>00</sub> mode laser ( $X/\sigma \approx 1$ ) at 27.4 GPa, while the black bold curve is from a sample heated by TEM<sub>01</sub> mode laser ( $X/\sigma \approx 0.5$ ) at 35.5 GPa. The 27% greater width of the gray curve, relative the black curve, can be explained entirely by the greater temperature gradients in the x-ray volume. Thin curves are for a model of diffraction-peak shapes assuming an isothermal peak width of 0.02 Å, as measured from postheating x-ray diffraction.

with both determinations lower than the actual pressure (by 7%–12%).

Viewed in another way, considering a sample with an accurate pressure determination the systematic error in volume determination causes an error of up to 100% in the inferred thermal expansion. For instance, under the conditions of Fig. 5(a) (case B; temperature condition I), the volume for gold at 20 GPa and 3000 K would be overestimated by 1.3%, leading to an overestimate of the average (300–3000 K) thermal expansivity by  $5 \times 10^{-6} \text{ K}^{-1}$ , a discrepancy of about 40%.

## COMPARISON WITH DATA

Figure 7 shows energy-dispersive x-ray diffraction data collected at the GSECARS beamline 13-IDD. The sample of interest (a mixture of oxides) was insulated from the diamonds using polycrystalline MgO layers and heated to the same peak temperature, 2150 ( $\pm 75$ ) K, but using two different laser modes for heating, thereby varying the  $X/\sigma$  ratio. Both diffraction patterns were taken with the same x-ray beam dimension ( $X \approx 10 \mu\text{m}$ ), yet the data collected using a TEM<sub>00</sub> mode ( $\sigma = 8 \mu\text{m}$ ) at 27.4 GPa is 27% wider than the peak collected using a TEM<sub>01</sub>\* heating mode ( $\sigma = 15 \mu\text{m}$ ) at 35.5 GPa. Given the peak positions, the pressures inferred from these diffraction lines would be 27.1 and 35.1 GPa, respectively (systematic errors of 0.3 and 0.4 GPa). While different sample loadings, each of the diffraction patterns is from the end of a heating cycle and is therefore assumed to be for an annealed sample. Indeed, both samples exhibit a MgO peak width full width at half maximum (FWHM) of 0.02 Å after heating [to peak temperatures of 2300 ( $\pm 90$ ) K and 2500 ( $\pm 75$ ) K, respectively], comparable with the detector resolution of the energy-dispersive system (150 eV at 25 keV, or  $\delta E/E = \delta d/d = 0.6\%$ ). The present measurements are therefore insensitive to microshear strain within the insulation layers.

Forward modeling of the peak profiles show that the  $P-V$  relationship can be determined for the sample, given a known temperature distribution across the x-ray diffraction volume. Modeling the peak shapes assuming half thermal pressure and half thermal expansion conditions (case C), and a linear temperature distribution through the sample, reproduces the observed diffraction lines (Fig. 7). While no peak splitting or shoulders are observed, the diffraction peaks are slightly asymmetric in accord with the model calculations. Data collected from a system with better resolution will be required in order to measure the predicted peak shapes in detail.

### EFFECT OF THE DEBYE-WALLER TEMPERATURE FACTOR

An additional complication of x-ray diffraction measurements from samples under temperature gradients is the effect of the Debye-Waller temperature factor, which predicts a decreasing intensity of diffraction due to increasing amplitudes of atomic vibrations (i.e., less coherent scattering) with increasing temperature.<sup>18</sup> The Debye-Waller factor is applied directly to the intensity of the diffraction peak

$$I = I_0 e^{-2M}, \tag{19}$$

where  $I$  is the intensity of the peak,  $I_0$  is the intensity at 0 K and, for cubic materials,  $M$  is

$$M = \frac{6h^2 T}{mk\Theta^2} \left[ \phi(x) + \frac{x}{4} \left( \frac{\sin \theta}{\lambda} \right)^2 \right], \tag{20}$$

where  $h$ ,  $k$ ,  $m$ ,  $\theta$ , and  $\lambda$  are Planck's constant, Boltzman's constant, mass of the atom, diffraction angle and wavelength, respectively, with  $x = \Theta/T$ . The function  $\phi(x)$  is

$$\phi(x) = \frac{1}{x} \int_0^x \frac{\xi}{e^\xi - 1} d\xi \tag{21}$$

and can be evaluated through series solutions.<sup>19</sup>

The Debye-Waller effect depends on pressure through the volume dependence of the Debye temperature [Eqs. (16)–(18)]. Over the temperature range possible within the diffraction volume, the effect of the Debye-Waller factor can be significant: up to 60% variation in  $I/I_0$  for gold. However, the pressure effects are much smaller, because the pressure variations within the hotspot are smaller, such that even in the most extreme case of isochoric conditions, the Debye-Waller factor only varies by  $\sim 10\%$  or less, due to pressure variations across the sample.

Figure 8 illustrates the effect on the inferred peak shape for gold of the case involving full thermal expansion of the sample [viz. Fig. 4(b)], showing the additional effect that inclusion of the Debye-Waller factor has on the calculated diffraction line for gold. Because the intensity of diffraction is greater at low temperatures, the low-temperature end of the diffraction curve is emphasized but the general peak shape is unchanged.

X-ray diffraction is more sensitive to those parts of the x-ray volume that are at lower temperature for two reasons. The first is the cylindrical symmetry of the hotspot (Fig. 2), which preferentially weights diffraction from large-radius

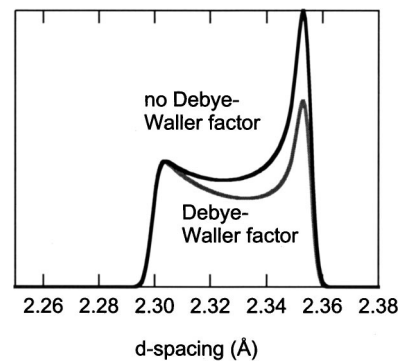


FIG. 8. Effect of the Debye-Waller factor on a diffraction-peak shape (gray) compared with the predicted peak shape assuming a constant Debye-Waller factor over the temperature range in the x-ray volume (black) for case B and condition I. The Debye-Waller factor acts to decrease intensity at high  $d$  spacings, corresponding to the hotter portions of the sample, relative to low  $d$  spacings.

values (hence, lower temperatures). Put simply, a larger fraction of the x-ray diffraction volume within the sample is at lower rather than higher temperatures. The second reason is the greater diffraction intensity of the crystal at lower temperatures due to the Debye-Waller factor. Therefore, both the geometrical and thermal effects cause the x-ray diffraction measurement to be more sensitive to the lowest (rather than the highest) temperatures in the x-ray diffraction volume. In an effort to quantify this effect, a weighted average temperature of the x-ray diffraction volume is defined. If each point of the sample volume is then weighted by the Debye-Waller factor, we can define a weighted average temperature according to the intensity of x rays coming from each point within the diffraction volume

$$\overline{T}_w = \frac{\int_0^D \int_0^X e^{-2M} T(r,z) r dr dz}{\int_0^D \int_0^X e^{-2M} r dr dz}, \tag{22}$$

where  $T(r,z)$  is defined by Eq. (6) or (7).

For each material, the geometrically averaged temperatures ( $e^{-2M} = 1$ ; unweighted) are systematically larger than the weighted averages, reflecting the fact that the x-rays are preferentially diffracted from the lower-temperature regions of the sample (Fig. 9). Those geometries with the smallest temperature variations are less affected by such a phenomenon; however, the present models are an idealization, and no sample is likely to have such small temperature variations. When combining the temperature variation across the sample with the Mie-Grüneisen equation of state, the differences in inferred temperature affect the inferred pressure of the sample, potentially resulting in errors in assessing the equation of state or phase boundary of the sample. Figure 9 (right side) shows that the effect on the inferred pressure of this difference in temperature is systematic, though smaller in magnitude than the influence of peak shapes due to the thermal expansion effects discussed earlier.

### SUMMARY

The models presented here illustrate some of the factors that must be included in the analysis of x-ray diffraction patterns taken from the laser-heated diamond cell (i.e., in the

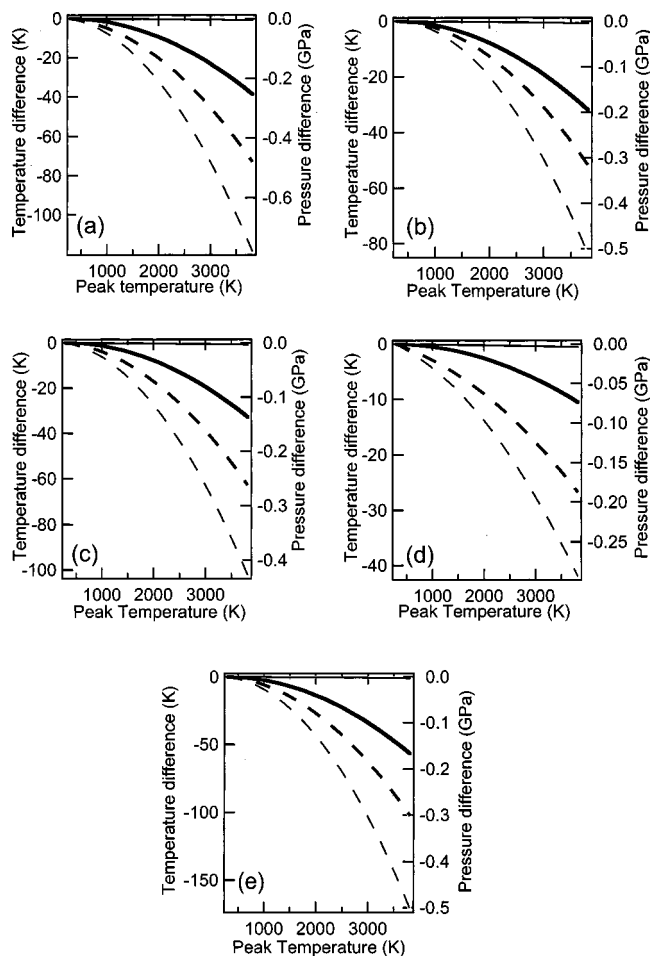


FIG. 9. Difference between the volume-average temperature and the volume-average temperature weighted by the Debye–Waller factor [Eq. (22)], and corresponding pressure differences inferred from calibration standards: (a) Pt; (b) Au; (c) MgO; (d) diamond; and (e) NaCl. Bold lines are for  $X=\sigma$  and thin lines are for  $X=\sigma/4$ , whereas solid lines indicate perfect axial insulation and dashed lines indicate no insulation layers.

presence of temperature gradients). Even in the ideal case of small radial gradients and no axial gradients in temperature, the pressures inferred for a sample can differ from the actual pressure by as much as 20%. In addition, for samples containing materials with distinctly different thermoelastic properties, the inferred pressures would be expected to differ from each other because the temperature to which each material is most sensitive is different. Therefore, when measur-

ing the relative equations of state of materials, for example of a sample relative to a standard, it is crucial to take into account the temperature distribution and its effects on the diffraction pattern. Given the models presented here, the best internal standards for a particular experiment are those with thermoelastic parameters as similar as possible to those of the sample of interest.

- <sup>1</sup>R. Jeanloz and A. Kavner, Phys. Trans. R. Soc. London **354**, 1279 (1995).
- <sup>2</sup>F. Birch, J. Geophys. Res. **83**, 1257 (1978).
- <sup>3</sup>A. Kavner and T. Duffy, J. Appl. Phys. **89**, 1907 (2001).
- <sup>4</sup>S. Bodea and R. Jeanloz, J. Appl. Phys. **65**, 4688 (1989).
- <sup>5</sup>M. Manga and R. Jeanloz, *Properties of Earth and Planetary Materials at High Pressure and Temperature* (American Geophysical Union, Washington, DC, 1998), pp. 17–25.
- <sup>6</sup>A. Dewaele, G. Fiquet, and P. Gillet, Rev. Sci. Instrum. **69**, 2421 (1998).
- <sup>7</sup>W. Panero and R. Jeanloz, J. Geophys. Res. **106**, 6493 (2001a).
- <sup>8</sup>W. Panero and R. Jeanloz, Rev. Sci. Instrum. **72**, 1306 (2001b).
- <sup>9</sup>G. Shen, M. L. Rivers, Y. Wang, and S. R. Sutton, Rev. Sci. Instrum. **72**, 1273 (2001).
- <sup>10</sup>L. S. Dubrovinsky, S. K. Saxena, P. Lazor, and H.-P. Weber, Structure of  $\beta$ -iron at High Temperature and Pressure, Science, [www.sciencemag.org/cgi/content/full/281/5373/11a](http://www.sciencemag.org/cgi/content/full/281/5373/11a), 1998.
- <sup>11</sup>D. L. Heinz, Geophys. Res. Lett. **17**, 1161 (1990).
- <sup>12</sup>H.-K. Mao, G. Shen, R. J. Hemley, and T. S. Duffy, *Properties of Earth and Planetary Materials at High Pressure and Temperature* (American Geophysical Union, Washington, DC 1998), pp. 27–34.
- <sup>13</sup>S. H. Shim, T. S. Duffy, and G. Shen, Nature (London) **411**, 571 (2001).
- <sup>14</sup>A. Kavner, T. Duffy, D. Heinz, and G. Shen, EOS Trans. Am. Geophys. Union **79**, S163 (1998).
- <sup>15</sup>J. C. Jamieson, J. N. Fritz, and M. H. Manghnani, in *High Pressure Research in Geophysics*, edited by S. Akimoto and M. H. Manghnani (Center for Academic Publications, Tokyo, 1982), pp. 27–48.
- <sup>16</sup>D. Andrault *et al.*, Science **278**, 831 (1997).
- <sup>17</sup>G. Fiquet, D. Andrault, J. P. Itié, P. Gillet, and P. Richet, Phys. Earth Planet. Inter. **95**, 1 (1996).
- <sup>18</sup>B. D. Cullity, *Elements of X-ray Diffraction*, 2nd ed. (Addison-Wesley, Reading, MA, 1978).
- <sup>19</sup>M. Abramowicz and I. A. Stegun, *Handbook of Mathematical Functions* (Dover, Mineola, NY, 1970).
- <sup>20</sup>N. C. Holmes, J. A. Moriarty, G. R. Gathers, and W. J. Nellis, J. Appl. Phys. **66**, 2962 (1989).
- <sup>21</sup>D. L. Heinz and R. Jeanloz, J. Appl. Phys. **55**, 885 (1984).
- <sup>22</sup>I. Jackson and H. Niesler, in *High Pressure Research in Geophysics*, edited by S. Akimoto and M. H. Manghnani (Tokyo, 1982), pp. 93–114.
- <sup>23</sup>I. V. Alexandrov, A. F. Goncharov, A. N. Zisman, and S. M. Stishov, Sov. Phys. JETP **66**, 384 (1987).
- <sup>24</sup>Y. Sato-Sorensen, J. Geophys. Res. **88**, 3543 (1983).
- <sup>25</sup>O. L. Anderson and D. G. Isaak, in *Mineral Physics and Crystallography: A Handbook of Physical Constants*, edited by T. J. Ahrens (American Geophysical Union, Washington, DC, 1995).
- <sup>26</sup>C. Kittel and H. Kroemer, *Thermal Physics*, 2nd ed., (W. H. Freeman and Company, New York, 1980).